SEMARAK ILMU PUBLISHING

Journal of Advanced Research in Applied Mechanics

Journal homepage:
https://semarakilmu.com.my/journals/index.php/appl_mech/index
ISSN: 2289-7895

Model Predictive Current Control Fed by Single- Phase Indirect Matrix Converter (SP-IMC) with Reactive Power Minimization

Hazrul Mohamed Basri[1], Kasumawati Lias[1,*], Yonis M Yonis Buswig[1], Saad Mekhilef[2]

[1] Department of Electrical and Electronics Engineering, Faculty of Engineering, Universiti Malaysia Sarawak (UNIMAS), Kota Samarahan, Sarawak, Malaysia
[2] School of Engineering, Swinburne University of Technology, Melbourne, Australia

ARTICLE INFO

Article history:
Received 25 May 2025
Received in revised form 27 June 2025
Accepted 4 July 2025
Available online 15 July 2025

Keywords:
Euler's formulation; single-phase indirect matrix converter; model predictive control; reactive power minimization; robustness test

ABSTRACT

This study presents a predictive current control and reactive power minimization strategy for a two-level single-phase indirect matrix converter (SP-IMC). The proposed control strategy takes advantage of the discrete nature of the system to predict the future load current and reactive power behaviour to perform switching optimization based on a minimum cost function criterion. Forward Euler's approximation is used based on unitary power factor condition, minimum reactive power, and minimum load current harmonic content (THD%). An optimized rectifier switching strategy was also conducted to ensure positive fictitious dc-link voltage at any instant. Several robustness tests have been conducted at a laboratory scale and the experimental results of the proposed control are provided in this paper. From the experimental results, the Forward Euler's approximation exhibits good load current reference tracking and reactive power minimization ability.

1. Introduction

The ac-ac power conversion is synonymous to applications such as renewable-energy [1], adjustable speed drive [2,3] and many others. There has been intensive research with three phase direct and indirect matrix converters [4–7]. However, the single-phase indirect matrix converter is lacking of literature. With this topology, a single-phase device can be used by tapping from a three-phase network. The application of single phase covers a wide range of application such as residential, and rural areas. Some concrete industrial examples of three phase to single phase conversions are the battery charging using wireless power transfer [8], electric vehicles and railway traction system [9]. In fact, most of the electrical appliances rely on single phase connection like computer-related equipment, basic lightings, and other power electronics devices [10].

There are a number of different topologies for direct ac-ac converters. Three major topologies to convert from ac to ac such as cycloconverter, back to back power converter (ac- dc-ac converter) and lastly matrix converter. The major drawback of cycloconverter is the substantial harmonics

* *Corresponding author.*
E-mail address: lkasumawati@unimas.my

https://doi.org/10.37934/aram.140.1.4459

pollution due to irregular and fast commutating semiconductor switching [11,12]. Meanwhile, back to back power converter, it has a nearly similar physical structure as the indirect matrix converter. It combines rectifier and inverter via intermediate dc-link element. Most of the back to back power converter considers naturally commutated semiconductor switches to synthesize the positive dc link voltage. As a consequence, a bidirectional power flow cannot be attained [13]. The existence of the dc- link capacitor requires regular maintenance because this element is susceptible to grid disturbances. Furthermore, for middle-range voltage, the size of the capacitor is huge and bulky which affect the size and volume of the power circuit. Another variant of single phase ac-ac converter is the direct matrix converter [14]. The total number of semiconductor switches is the major drawback of this topology. Recently, indirect matrix converter has gained special attention due to its compact size, reliability and performance. For this salient feature, matrix converter is now becoming a good alternative to back-to-back power converter and cycloconverter. IMC has superiority in terms of reliability, durability and compactness of size and volume. IMC topology has been widely discussed, and many researchers have developed various IMC topologies suitable for specific applications [15–17].

There are many modulation strategies for IMC. The initial establishment of matrix converter modulation scheme was PWM based algorithm presented in [18,19] by Alesina and Venturini for direct matrix converter. This modulation technique features controllable output voltage, adjustable input power. However, the achievable voltage ratio transfer was limited to only 0.5. The most relevant variety of PWM modulation is the Carrier-Based PWM (CB-PWM) as reported in [20,21]. The carrier signal for the rectifier to drive the circuit is a symmetrical triangular signal of constant frequency, while the carrier for the inverter is a triangular waveform with variable rising and falling edge slope, the real time calculation of the slope requires high computational cost to the controller. Besides PWM, SVM gain popularity due to its intuitive concept and superiority of performance compared to the PWM. The space vector modulation PWM (SVPWM) method has been generally used to control the IMC because it has a good performance such as lower current harmonics and controllable switching frequency. However, the computational requirement for this control is extremely high, and the control modelling is very complex. These control mentioned above does not directly feature reactive power minimization. The inclusion of reactive power minimization with this control strategy is at the expense of high computational cost.

In this paper, the author has implemented finite control set model predictive control (FCS-MPC) with reactive power minimization and assert the performance of SP-IMC. FCS-MPC has been successfully implemented for various topologies due to its simplicity and reliability as recorded in [22–27]. Moreover, this scheme does not require internal current control loops and modulators, which greatly reduces its complexity. Unlike space vector modulation strategy, the control strategy allows the use of all valid switching states including the rotating vectors [11,28]. This technique has been successfully applied to a wide range of power converters topologies. The predictive control is actually an optimization algorithm. In order to work out this strategy, it has to be implemented in digital microprocessor. Therefore, an obvious starting point of the analysis is to perform discrete mathematical analysis [29]. Subsequently, the same discrete mathematical models of the power converter, input filter and load are used to predict the future behavior of the load current and reactive power for each valid switching state. In our case, 12 switching combination are considered [30]. The optimization task is undertaken by a cost function which characterises the control objectives. The main function of the cost function is to select the switching combination that minimizes the reference tracking error and minimizes the predicted reactive power value. After calculating the optimum switching combination, they will be applied to the next sampling time.

2. Single Phase Indirect Matrix Topology

The proposed power circuit englobes three main circuits as illustrated in Figure 1. Firstly, a second-order input filter which contains three elements, resistive and inductive elements are connected in series with the input voltage supply meanwhile, the capacitive elements are connected as a star connected circuit. The main task of the input filter is to perform high-order harmonic mitigation from the three- phase ac supply and also served as protection from over voltage cases. The voltage across the input filter capacitor is fed to the second circuit which is the bidirectional front- end rectifier. The main function of this power circuit is to synthesize a positive dc-link voltage. Finally, conventional H-Bridge inverter circuit composed by four switching devices is used to convert the dc-link voltage into ac voltage across the load. Both the rectifier and inverter circuits are connected without any physical dc-link elements. The absence of the dc energy storage element enables a more compact design of the converter.

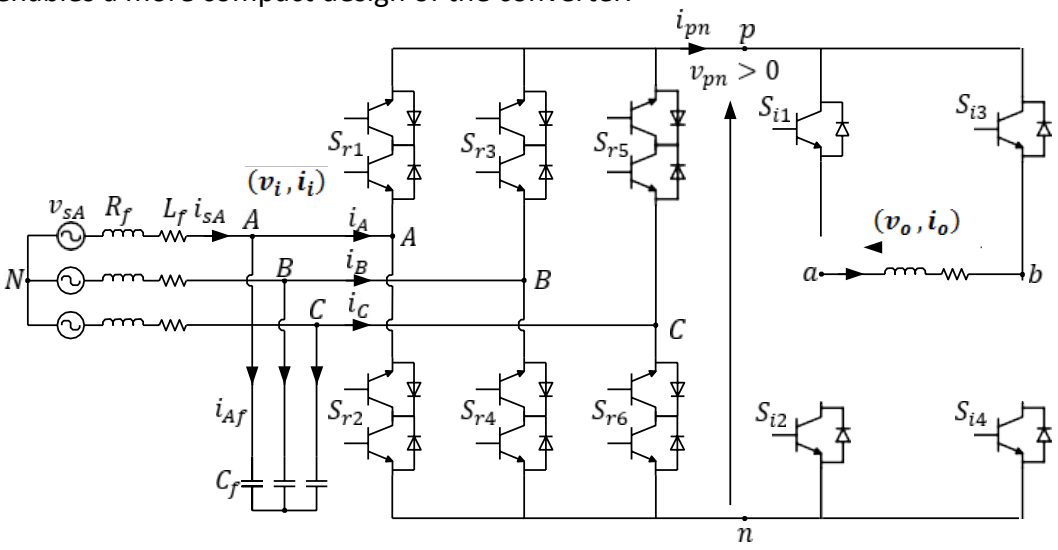

Fig. 1. Single phase indirect matrix converter topology

2.1 Rectifiers

The rectifier can form nine distinct switching possibilities. At any instant, all switching combinations can be equally divided into 3 groups corresponding to positive, negative and zero dc-link voltage. Properly switching of one upper-level rectifier switch simultaneously with one lower level rectifier switch enables the rectifier to generate positive dc-link voltage. The switching combinations which contribute to the positive dc-link voltage are selected beforehand using optimal rectifier switching selection proposed in subsequent sections. In order to avoid short circuit of the dc-link, the following switching constraints are imposed Eq. (1) and Eq. (2):

$$\sum_{k=0}^{2} S_{r(1+2k)} = 1\,,\ \sum_{k=0}^{2} S_{r(2+2k)} = 1 \tag{1}$$

$$S_{r(1+2k)} \cdot S_{r(2+2k)} = 0,\ k = \{0,1,2\} \tag{2}$$

Eq. (3) expresses the relationship between the input current as a function of the dc-link current and rectifier switches.

$$i_i = \begin{bmatrix} S_{r1} - S_{r2} \\ S_{r3} - S_{r4} \\ S_{r5} - S_{r6} \end{bmatrix} i_{PN} \tag{3}$$

Eq. (4) expresses the dc-link voltage as a function of rectifier switch states and the input voltage. The selected line to line voltage is reflected to the dc-link terminals to create positive potential difference.

$$v_{PN} = [S_{r1} - S_{r2} \quad S_{r3} - S_{r4} \quad S_{r5} - S_{r6}] \begin{bmatrix} v_A \\ v_B \\ v_C \end{bmatrix} \tag{4}$$

2.2 Optimized Rectifier Switching Strategy

By considering six possible switching states of the rectifier and four allowable switching combination of the inverter, a total of (6x4) 24 possible switching states can be counted. However, as explained earlier, only three of the possible rectifiers switching states can synthesize positive dc-link voltage. If the three plausible switching combination can be selected beforehand, there will be a possibility to reduce the computational cost in a significant manner. To ensure positive dc-link voltage, the input voltage connected to the positive terminal of the dc-link should be greater than the one connected to the negative terminal. The vector position can be divided into six groups namely sextant 1 to 6 as shown in Table 1. Each group has specific angle and allowable rectifier switching.

Table 1
Sector and Angle Classification

sextant	$\theta^\circ = \frac{180^\circ}{\pi} \times tan^{-1}\left(\frac{\sqrt{3}(v_B^k - v_C^k)}{2v_A^k - v_B^k - v_C^k}\right) + 180^\circ$	Vector position			Allowed rectifier switching S_{ri}
		min	med	max	i
1	$0 \le \theta < 60$	v_A	v_B	v_C	$i = \{(2,5)\ (4,5)\ (2,3)\}$
2	$60 \le \theta < 120$	v_B	v_A	v_C	$i = \{(4,5)\ (2,5)\ (1,4)\}$
3	$120 \le \theta < 180$	v_B	v_C	v_A	$i = \{(1,4)\ (1,6)\ (4,5)\}$
4	$180 \le \theta < 240$	v_C	v_B	v_A	$i = \{(1,6)\ (1,4)\ (3,6)\}$
5	$240 \le \theta < 300$	v_C	v_A	v_B	$i = \{(3,6)\ (2,3)\ (1,6)\}$
6	$300 \le \theta < 360$	v_A	v_C	v_B	$i = \{(2,3)\ (3,6)\ (2,5)\}$

2.3 Inverters

At the inversion stage, all four unidirectional inverter switches can form four possible switching combinations. Here, the upper-level switches work in complimentary to the lower-level inverter switches as described in Eq. (5). These switching constraints are imposed due to the inductive nature of the load. Improper switch would draw high current to the load and destroy the system. Eq. (6) expresses the relationship between the dc-link current with the load currents. For single phase IMC topology, the load voltage of the inverter can be expressed in Eq. (7).

$$S_{i(1+2l)} + S_{i(2+2l)} = 1\,,\ l = \{0,1\} \tag{5}$$

$$i_{PN} = (S_{i1} - S_{i3})i_o \tag{6}$$

$$v_o = (S_{i1} - S_{i3})v_{PN} \tag{7}$$

3. Discretization Strategy

In this section, two sub-topics will be discussed. Firstly, the theoretical approach of the discrete mathematical modelling of the input filter will be elaborated. Eq. (8) represents the forward Euler's approximation. The superscripts indicate the instantaneous value meanwhile indicate the one step predicted value.

$$x^{k+1} = x^k + T_s.f(x^k, u^k) \tag{8}$$

An input filter is placed on the input side for two main purposes. First is to avoid over-voltages and secondly is to mitigate the harmonic distortion caused by the commutations. The dynamic behaviour of the input filter can be written as a function of the filter capacitor voltage, filter inductor current and load current as indicated in Eq. (10) and Eq. (11). Eq. (12) expresses the one step prediction of input voltage and supply current.

$$\frac{d}{dt}\begin{bmatrix} v_i \\ i_s \end{bmatrix} = A\begin{bmatrix} v_i \\ i_s \end{bmatrix} + B\begin{bmatrix} v_s \\ i_i \end{bmatrix} \tag{9}$$

$$A = \begin{bmatrix} 0 & {}^{1}/_{C_f} \\ -{}^{1}/_{L_f} & -{}^{R_f}/_{L_f} \end{bmatrix},\ B = \begin{bmatrix} 0 & -{}^{1}/_{C_f} \\ {}^{1}/_{L_f} & 0 \end{bmatrix} \tag{10}$$

$$\begin{bmatrix} v_i^{k+1} \\ i_s^{k+1} \end{bmatrix} = \phi\begin{bmatrix} v_i^k \\ i_s^k \end{bmatrix} + \Gamma\begin{bmatrix} v_s^k \\ i_i^k \end{bmatrix} \tag{11}$$

where

$$\phi \approx e^{A.T_s} = \begin{bmatrix} a_{11} & a_{12} \\ a_{21} & a_{22} \end{bmatrix} \tag{12}$$

$$\Gamma \approx A^{-1}(\phi - I_{2\times 2}).B = \begin{bmatrix} b_{11} & b_{12} \\ b_{21} & b_{22} \end{bmatrix} \tag{13}$$

Before expressing the load current prediction, the continuous differential expression representing the load voltage and load current Eq. (14) should be discretized to include the sampling time.

$$\frac{di_o}{dt} = \frac{1}{L}v_o - \frac{R}{L}i_o \tag{14}$$

For ease of analysis, three parameters and will be introduced. These parameters are entirely dependent on the switching states of the rectifier and inverter circuits as dictated by (15).

$$k_1 = (S_{i1} - S_{i3})(S_{r1} - S_{r2})$$

$$k_2 = (S_{i1} - S_{i3})(S_{r3} - S_{r4}) \tag{15}$$

$$k_3 = (S_{i1} - S_{i3})(S_{r5} - S_{r6})$$

Eq. (16) describes the one-step prediction of the load current using forward Euler's approximation. There is a necessity to acquire several instantaneous values of load current, supply voltage, supply current and input voltage to calculate the predicted value of load current. Dedicated current and voltage transducers circuits had been designed to acquire these variables. Considering the load current as controlled variable and input voltage as input, the predicted values of load current can be described as:

$$i_o^{k+1} = \left(1 - \frac{T_s R}{L}\right) i_o^k + \frac{T_s}{L}[k_1 \quad k_2 \quad k_3]\, v_i^k \tag{16}$$

The proposed predictive control features reactive power minimization ensuring nearly unity power factor operation. Similar to load current, the reactive power must be converted into a discrete format. The calculation of predicted reactive power is given in Eq. (17) where α and β denotes the active and reactive components respectively.

$$Q_s^{k+1} = v_{s\alpha}^k i_{s\beta}^{k+1} - v_{s\beta}^k i_{s\alpha}^{k+1} \tag{17}$$

Considering significantly small sampling time, it is possible to assume Eq. (18).

$$v_s^{k+1} \approx v_s^k \tag{18}$$

4. Predictive Current Control and Strategy

In this section, the prediction model of the system is reviewed. For that purpose, the converter needs to be expressed in a mathematical format. In this case, the load voltage and input current should be expressed as a function of all possible commutation states. The following subsection discusses the relevant mathematical equations related to the SP-IMC topology. The proposed model predictive control involves four simple steps.

i. Measure the initial variable - load current, supply voltage and supply current.
ii. Determine the sextant of the input voltage.
iii. Compute the cost function using predicted value of load current and reactive power. The calculation of the cost function should be iterated 12 times corresponding to the 12 possible switching combinations.
iv. Select the switching combination giving the minimal cost function and apply them at the next sampling time.

4.1 Cost Function

The performance of predictive control lies in the optimization of the cost function. In this paper, the cost function determines the tracking error for all 12 possible switching states. The optimal switching states that will be applied for the next sampling time correspond to the one that compute the least tracking error. This can be mathematically translated into minimum cost function. Listed below are three control requirements:

i. Load current reference tracking ability
ii. Minimum reactive power
iii. Positive fictitious dc-link voltage

Control requirement 1 and 2 will be handled by the cost function. For control requirement 3, the issue of ensuring positive dc-link voltage has been handled by the proposed rectifier switching strategy in section 2. The control requirement 1 and 2 are defined as a sum of two sub-cost function g_1 and g_2. g_1 represents the load current reference tracking error and defined as Eq. (19).

$$g_1 = \left| i_o^{ref} - i_o^{k+1} \right| \tag{19}$$

Meanwhile g_2 in Eq. (20) represents the predicted reactive power. This quantity will be compared to the reference reactive power which in this case equal to zero.

$$g_2 = Q^{k+1} \tag{20}$$

Lastly, the final cost function g is defined as a linear combination of g_1 and g_2 as shown in Eq. (21). is associated with a weighting factor λ_Q because g_1 and g_2 are not in the same nature. The weighting factor λ_Q enable the conversion from VAR to A and brings g_2 to similar logarithmic scale as g_1.

$$g = g_1 + \lambda_Q |g_2| \tag{21}$$

4.2 Selection of T_S and λ_Q

In this work, the selection of these two parameters must comply with the primary objectives of this control, which are an outstanding load current reference tracking and minimization of reactive power. So far, the rules of selecting these parameters remained unclear. The common practice, an empirical approach is adopted. The normalized current error as in Fig.3 is plotted as a mesh graph by considering weighting factor and sampling time as *x* and *y*-axis respectively. As it can be anticipated, the normalized error recorded relatively insignificant error at small sampling time region. As the sampling time increases, the load current tends to deviate from the reference value. Another remarks from Figure 2 is that extreme value of the weighting factor also gives a negative impact to the reference tracking ability. Fig.3 depicts the effect of normalized reactive power to different values of sampling time and weighting factor.

$$\varepsilon_{io} = \left| i_o^{meas} - i_o^{ref} \right| \tag{22}$$

$$i_{o\,norm} = \frac{\varepsilon_{io} - \min(\varepsilon_{io})}{max(\varepsilon_{io}) - \min(\varepsilon_{io})} \tag{23}$$

$$\varepsilon_Q = \left| Q^{ref} - Q^{meas} \right| = |Q^{meas}| \tag{24}$$

$$Q_{norm} = \frac{\varepsilon_Q - \min(\varepsilon_Q)}{max(\varepsilon_Q) - \min(\varepsilon_Q)} \tag{25}$$

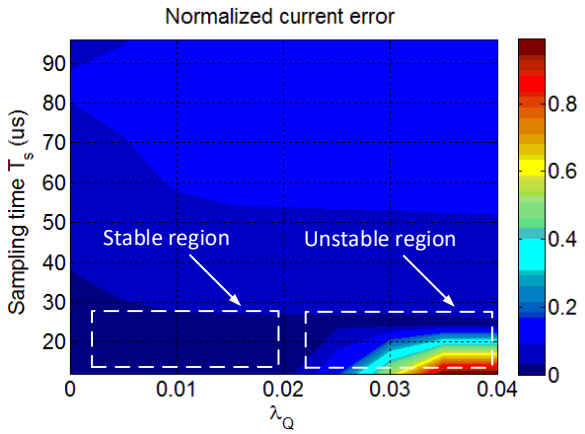

Fig. 2. Normalized current error

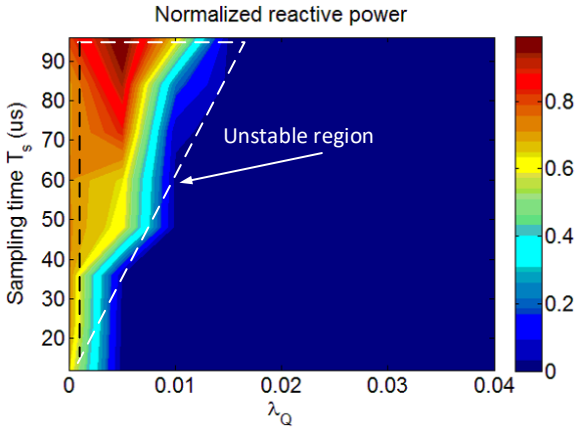

Fig. 3. Normalized reactive power

Finally, both Figure 2 and Figure 3 are combined into Figure 4 to find a stable region where it corresponds to the optimal value of the sampling time and reactive power. To conclude, the suitable pair of sampling time and weighting factor for the prepared experimental setup are located within the region of $T_s \in [20,40]\ \mu sec$ and $\lambda_Q \in [0.01,0.025]\ A/VAR$. It should be highlighted that the values given here might differ for different setup. Relative error and normalized current error are given by Eq. (22) and Eq. (23) respectively meanwhile Eq. (24) and Eq. (25) represents the relative reactive power error and its respective normalized error.

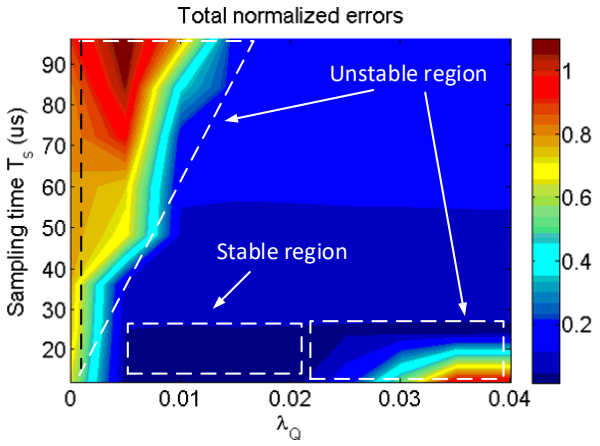

Fig. 4. Total normalized error

5. Experimental Results and Discussions

An experimental two-level single-phase indirect matrix converter (SP-IMC) prototype has been built in the laboratory. Figure 5 depicts the laboratory setup that was built for this project. A reconfigurable Xilinx Spartan 6–LX45 FPGA based controller was utilized for handling the control process. 12 switches for rectifier circuits and 4 Silicon Carbide MOSFET SCT2080KE switches for the H-Bridge circuit from ROHM Semiconductor was designed on a PCB board. Current sensor LEM LA25-NP and voltage transducers LEM LV-25-P are used to acquire the appropriate currents and voltages before sending to the ADC port. The scaling factor for the current and voltage transducers are fixed at $0.2V/A$ and 0.02 respectively. The topology circuit is powered by Chroma 61511 three phase ac supply which can deliver clean and balanced ac supply to the system. The ac supply was tuned to 30Vrms and 50Hz feeding the front end rectifier through a second order RLC filter. The FPGA board features 10 simultaneous $\pm 5V$ analogue input and four channel of $0/+5V$ analogue

output to display instantaneous variable such as reactive power. The reactive power is calculated from the FPGA board in real-time due to the absence of measuring device.

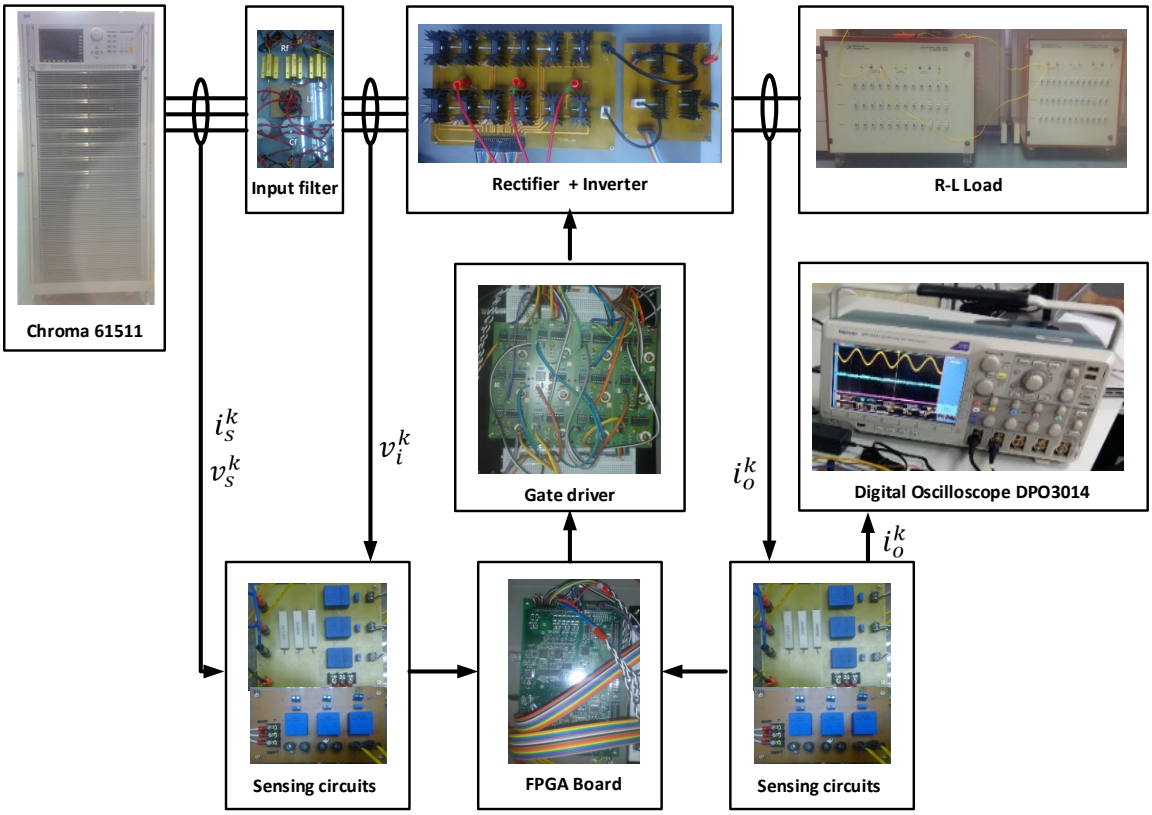

Fig. 5. Experimental setup

5.1 Experimental testing under normal condition

Three sets of results is provided to assert the behaviour of the load current with respect to different values of weighting factor λ_Q. Figure 6 displays the dynamic response of the load current, superimposed supply current with supply voltage and the instantaneous reactive power. This results is obtained without setting weighting factor ($\lambda_Q = 0\ A/VAR$). The main observation here is that the load current evolves as a sinusoidal signal replicating the reference load current given to the controller. The reference current is set to 2A peak to peak and fixed temporal frequency 50 Hz. The visible ripple and overshoot exhibited by the measured load current is significantly low. Without weighting factor, chaotic behaviour of supply current is observed. Arbitrary supply current spikes occurred during this test indicate that the system is performing without unity power factor condition.

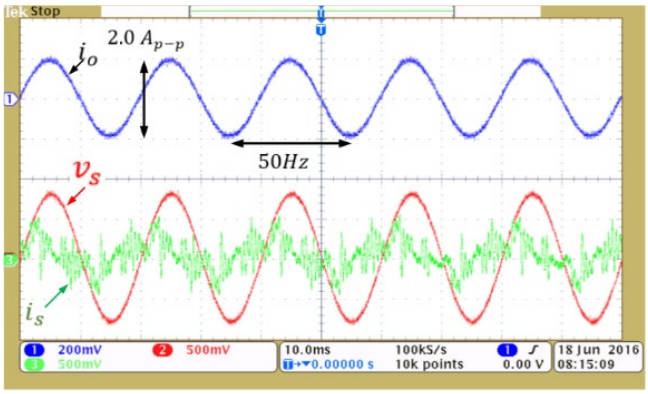

Fig. 6. Experimental results without weighting factor (1: Blue) Load current, (2: Red) Supply voltage, (3: Green) Supply current

Figure 7 and Figure 8 meanwhile exhibit the experimental results of the predictive current control for weighting factor $\lambda_Q = 0.01 A/VAR$ and $\lambda_Q = 0.025\ A/VAR$ respectively. As anticipated, the reference tracking quality of the load current slightly degraded when higher λ_Q is applied to the algorithm. A visible load current ripple start to develop while maintaining an acceptable distortion. The ability of load current tracking has been compromised by the reactive power minimization. As a results, a rise of THD% value could be observed but maintaining fairly a sinusoidal wave-shape because of the nature of the load. The R-L load combination give comparable effect as a low pass filter which reduce the high frequency components of the load current. With the inclusion of non-zero weighting factor, the power circuit starts to draw more orderly sinusoidal wave. Both supply current and supply voltage is now aligned in phase indicating that the system is now operating under unity power factor condition. A quantitative results is given in Table 4. The percentage current error is calculated offline after running the experiment. The error can be expressed as Eq. (26). The number of samples provided by the Textronix DPO 3014 Digital Phosphor Oscilloscope is n=10000 samples.

$$\%\varepsilon_i = \frac{\frac{1}{n}\sum_{k=1}^{n}\left|i_o^{ref} - i_o^{meas}\right|}{rms\left(i_o^{ref}\right)} \tag{26}$$

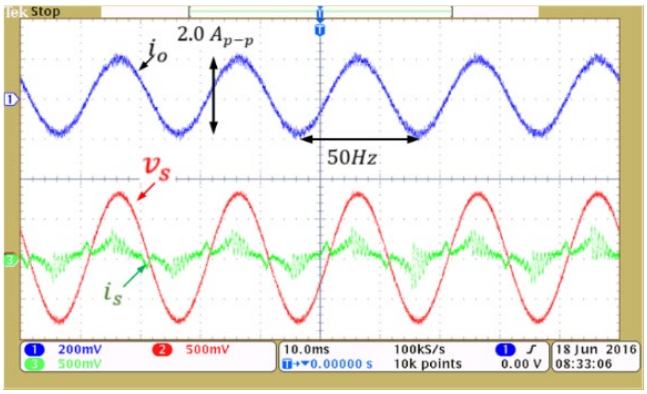

Fig. 7. Experimental results with $\lambda_Q = 0.01$ (1: Blue) Load current, (2: Red) Supply voltage, (3: Green) Supply current

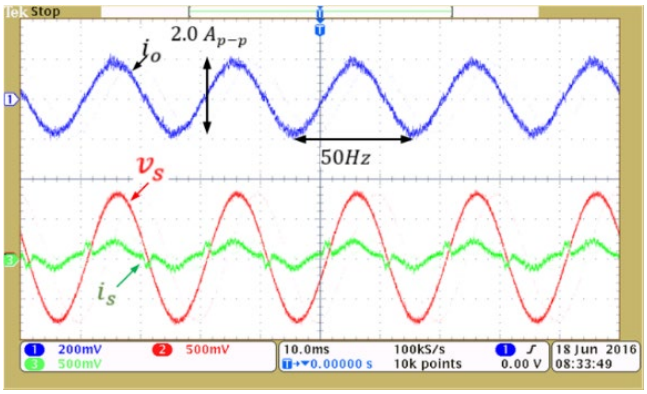

Fig. 8. Experimental results with $\lambda_Q = 0.025$ (1: Blue) Load current, (2: Red) Supply voltage, (3: Green) Supply current

Figure 9 and Figure 10 show the experimental reactive power for lambda $\lambda_Q = 0.01A/VAR$ and $\lambda_Q = 0.025A/VAR$ respectively. Due to the strong distortion of the supply current, an unwanted high reactive power is present on the input side $\lambda_Q = 0$. The maximum amplitude of the reactive power can reached up to 100 VAR. On the contrary, there is radical reduce of reactive power when $\lambda_Q = 0.025\ A/VAR$ is applied to the algorithm as can be observed in Figure 11. For both cases, the reactive power is pre-scaled and send to the analogue output with a fitting scale of $0.02\ V/VAR/div$.

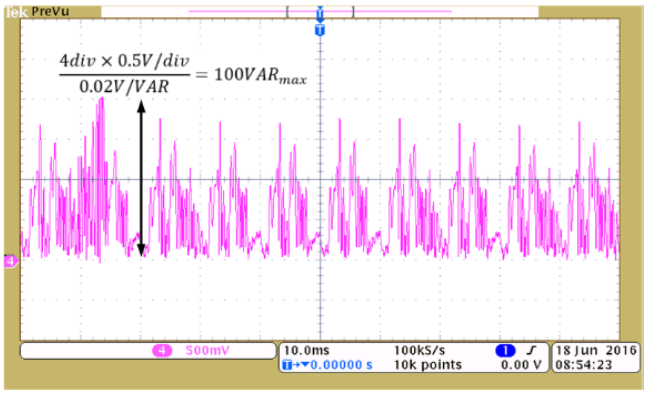

Fig. 9. Reactive power Q for $\lambda_Q = 0\ A/VAR$.

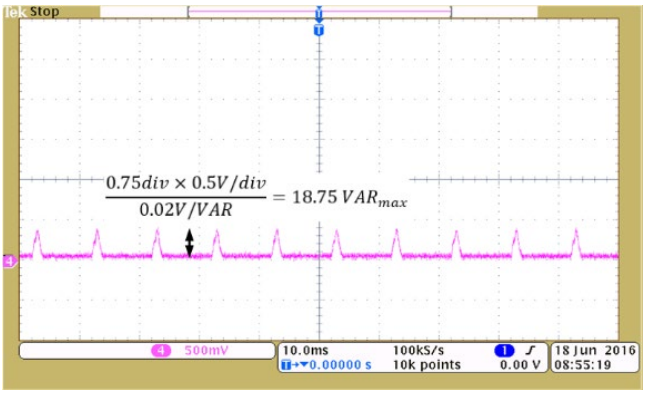

Fig. 10. Reactive power Q for $\lambda_Q = 0.025\ A/VAR$

5.2 Experimental testing under step and frequency change

First test consists of applying step changes as reference load current. In view of assessing the robustness, a step change and frequency change test has been conducted. Figure 11 shows the dynamics of the load current for step change test. The load current was initially set at 1A, 50 Hz and immediately, the load current amplitude is decreased to 0.5A. The weighting factor $\lambda_Q = 0.01$ remains unchanged during the whole experimental test. From this figure it can be observed that the load current ripple is slightly increased after the step change is applied. It should be noted that the optimal current amplitude for this test is 1A. The load current applied after the step change is considered under rated. This problem can be remediated by tuning the ac supply to a lower value to adjust the power required by the circuit.

Referring to Figure 11, the changes of amplitude took place in a very short transient period proof the reliability of the controller to detect sudden changes in the reference. Figure 12 shows the zoomed region of the transient period. It can be seen that the controller required 528.33 μsec to track the new value of the load current reference.

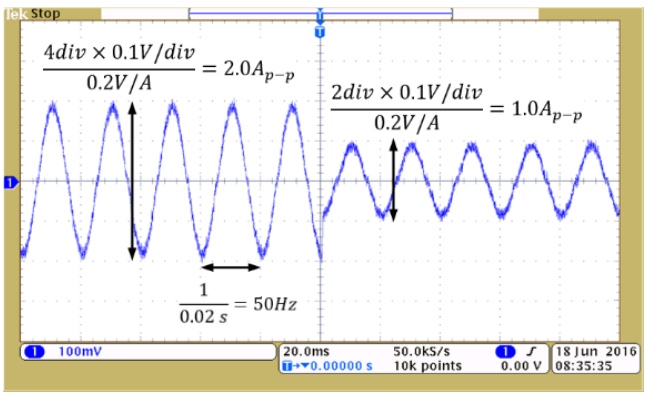

Fig. 11. Load current dynamic under step change test

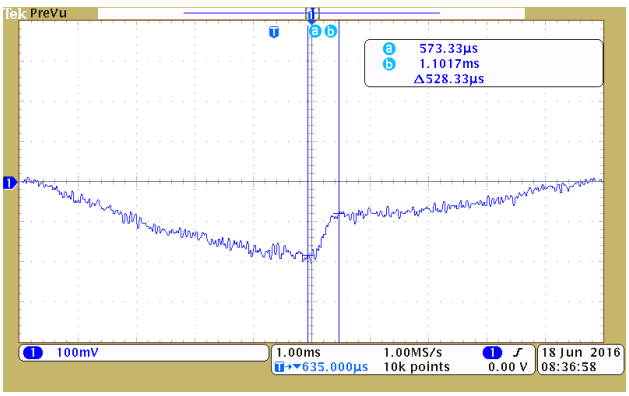

Fig. 12. Transient period for step change test

The fast tracking of the current reference confirmed extreme robustness of the proposed control against step changes. In the same philosophy, the proposed control is tested against frequency changes. For the frequency change test, the load current reference is fixed to 1A, 50 Hz and the frequency is changed to 100 Hz while remaining the same amplitude. Again, the measured load current is able to track reference changes and react to the changes within a short transient period as shown in Figure 13. The experimental setup has been tested for a frequency band ranging from 5 Hz to 155 Hz. Within this range, the controller is able to provide good load current reference tracking. Beyond this frequency range, the load current distorts and a non-sinusoidal wave can be observed. One of the drawbacks of the proposed control scheme is that, the switching frequency cannot be controlled. An additional cost function might be needed to control the switching frequency. The average switching frequency of this work is around 5.1 kHz. In order to widen the range of output frequency of the load current, higher switching frequency will be needed. Figure 14 displays the zoomed area during the transient of the load current. In case of frequency change, it took 608.33 μsec before converging to the reference value.

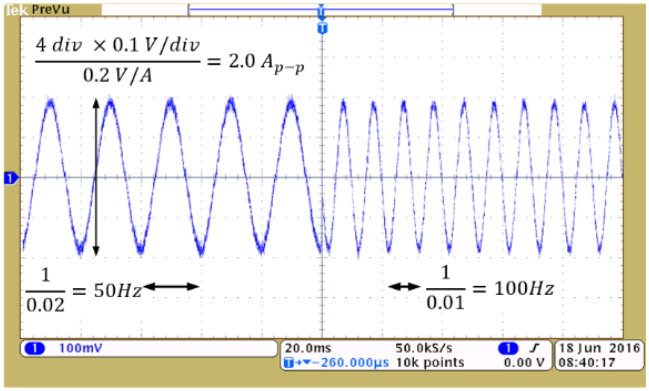

Fig. 13. Load current dynamic under frequency change test

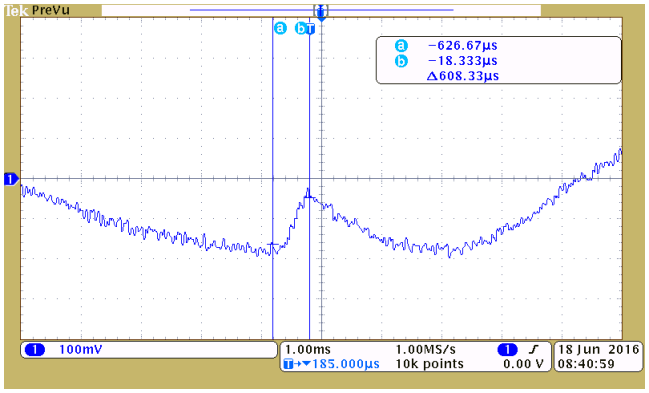

Fig. 14. Transient period for frequency change test

Figure 15 demonstrates the effectiveness of the rectifier switching strategy where at any instant, the dc-link voltage measured between the positive and negative terminal. This is important to ensure proper commutation of the h bridge. The value of the dc-link voltage is observed to be positive at any instant with upper and lower envelop are given by the line to line input voltage across the capacitor. Table 2 compares the performance of the different Euler's approximation for $\lambda_Q = 0\ A/VAR$ and $\lambda_Q = 0.01\ A/VAR$. This results reveal that the forward and Midpoint Euler's has been outperformed by the backward Euler's approximation. In fact, backward Euler's has the best trade-off between complexity and accuracy. Forward technique only considers the value of load current and load voltage at instant k.

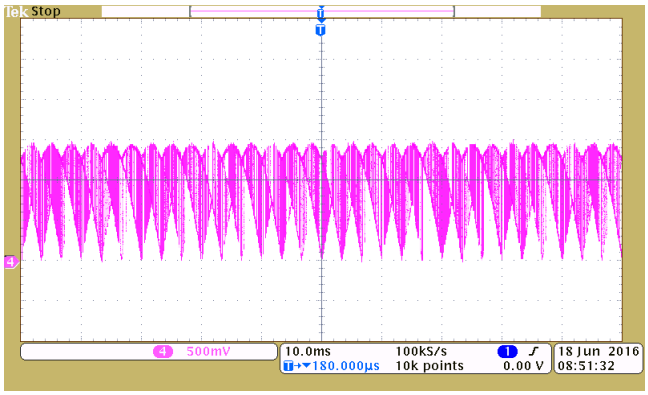

Fig. 15. Fictitious dc-link voltage

Despite being simple, it has the drawback of not having the knowledge of the predicted value of load voltage. On the other hand, midpoint Euler's formula is completely the reverse. For that reason, the controller board need to bear heavy computational burden and require longer time to compute the cost function due to the complex calculation.

Table 2
Performance evaluation for different approaches

$\lambda_Q = 0\ A/VAR$			$\lambda_Q = 0.01 A/VAR$		
THD (%)	$\%\varepsilon_i$	Q_{avg} (VAR)	THD (%)	$\%\varepsilon_i$	Q_{avg} (VAR)
4.27	6.19	25.04	4.93	8.10	2.04

Table 3 compares the performance of the proposed power circuit with different single phase ac/ac topology. In order to make fair comparison, [13] uses model predictive control to control the firing signal of the semiconductor switches.

Table 3
Comparisons with Relevant Literature

Evaluation criteria	Proposed	[13]	[14]
THD% (distortion)	3.63 ($\lambda_Q = 0$) 4.02 ($\lambda_Q = 0.01$)	2.87	2.80
Sampling time (μsec)	30	200	25
Robustness test	Yes	No	No
Reactive power minimization	Yes	No	No
Power flow	Bidirectional	Unidirectional	Bidirectional
Number of switches	10	8	12

Table 4 indicates the experimental parameters used in this paper.

Table 4
Experimental Parameters

Parameter	Symbol	Value
RMS supply voltage	V_s	$30\ V$
Supply frequency	f_s	$50\ Hz$
Filter resistance	R_f	$0.5\ \Omega$
Filter inductance	L_f	$420\ \mu H$
Filter capacitance	C_f	$25\ \mu F$
Output current amplitude	I_o	$0.5 - 1\ A$
Output frequency	f_o	$5 - 155\ Hz$
Load resistance	R	$24\ \Omega$
Load inductance	L	$46\ mH$
Sampling time	T_s	$30\ \mu sec$

6. Conclusions

In this paper, the predictive current control, reactive power minimization strategy and rectifier switching optimization strategy have been proposed to control a two-level single phase indirect matrix converter. The control strategy presented in this paper, based on predictive control, is much simpler and more intuitive than the classical methods used previously. The predictive control asserts a total of 12 possible commutation states and chose specifically the switching states that minimize the cost function. Several tests have been conducted to evaluate the robustness of the proposed control towards reference changes while the output currents continue to effectively track their references. For each test, low load current THD, low current ripple and ability to minimize the instantaneous reactive power are observed. By selecting proper sampling time and weighting factor, both reference tracking and reactive power minimization requirement can be fulfilled. From the experimental result, it was found that backward Euler's approximation exhibits better reference tracking performance, low total harmonics distortion and instantaneous reactive power compared to the other techniques.

Acknowledgements

The authors would like to acknowledge Universiti Malaysia Sarawak, Malaysia for the financial support provided to undergo this research under the project ID UNI/F02/RISE/85737/2023.

References

[1] Ghaffari, A., M. Krsti, and S. Seshagiri. "Power Optimization and Control in Wind Energy Conversion Systems Using Extremum Seeking." *IEEE Transactions on Control Systems Technology* 22, no. 5 (2014): 1684–1695. https://doi.org/10.1109/TCST.2014.2303112

[2] Ellabban, O., H. Abu-Rub, and B. Ge. "A Quasi-Z-Source Direct Matrix Converter Feeding a Vector Controlled Induction Motor Drive." *IEEE Journal of Emerging and Selected Topics in Power Electronics* 3, no. 2 (2015): 339–348. https://doi.org/10.1109/JESTPE.2014.2309979

[3] Boztas, G., S. Sünter, and O. Aydogmus. "Design of a Novel Single-Phase in Two-Phase Out Matrix Converter Driving an Induction Motor." *IET Power Electronics* 9, no. 7 (2016): 3191–3197. https://doi.org/10.1049/iet-pel.2015.0568

[4] Amini, J., R. Kazemzahed, and H. Madadi Kojabadi. "Performance Enhancement of Indirect Matrix Converter Based Variable Speed Doubly-Fed Induction Generator." *2010 1st Power Electronic & Drive Systems & Technologies Conference (PEDSTC)* (2010): 450–455. https://doi.org/10.1109/PEDSTC.2010.5471772

[5] Faraji, V., and D. Arab Khaburi. "A New Approach to DTC-ISVM for Induction Motor Drive System Fed by Indirect Matrix Converter." *2011 2nd Power Electronics, Drive Systems and Technologies Conference*. IEEE, February 2011, 367–372. https://doi.org/10.1109/PEDSTC.2011.5742448

[6] Ahmed, S. M., H. Abu-Rub, Z. Salam, and A. Kouzou. "Space Vector PWM Technique for a Novel Three-to-Seven Phase Matrix Converter." *IECON 2013 - 39th Annual Conference of the IEEE Industrial Electronics Society*. IEEE, November 2013, 4949–4954. https://doi.org/10.1109/IECON.2013.669993

[7] Raju, S., L. Srivatchan, and N. Mohan. "Direct Space Vector Modulated Three Level Matrix Converter." *2013 Twenty-Eighth Annual IEEE Applied Power Electronics Conference and Exposition (APEC)* (2013): 475–481. https://doi.org/10.1109/APEC.2013.6520252

[8] Weerasinghe, D. S. B., U. K. Madawala, D. J. Thrimawithana, and D. M. Vilathgamuwa. "A Three-Phase to Single-Phase Matrix Converter Based Bi-Directional IPT System for Charging Electric Vehicles." *2013 IEEE ECCE Asia Downunder - 5th IEEE Annual International Energy Conversion Congress and Exhibition, IEEE ECCE Asia 2013* (2013): 1240–1245. https://doi.org/10.1109/ECCE-Asia.2013.6579267

[9] Shu, Z., S. Xie, and Q. Li. "Single-Phase Back-to-Back Converter for Active Power Balancing, Reactive Power Compensation, and Harmonic Filtering in Traction Power System." *IEEE Transactions on Power Electronics* 26, no. 2 (2011): 334–343. https://doi.org/10.1109/TPEL.2010.2060360

[10] Sun, Q., J. Zhou, J. M. Guerrero, and H. Zhang. "Hybrid Three-Phase/Single-Phase Microgrid Architecture With Power Management Capabilities." *IEEE Transactions on Power Electronics* 30, no. 10 (2015): 5964–5977. https://doi.org/10.1109/TPEL.2014.2379925

[11] Rivera, M. et al. "A Comparative Assessment of Model Predictive Current Control and Space Vector Modulation in a Direct Matrix Converter." *IEEE Transactions on Industrial Electronics* 60, no. 2 (2013): 578–588. https://doi.org/10.1109/TIE.2012.2206347

[12] Kouro, S., P. Cortés, R. Vargas, U. Ammann, and J. Rodríguez. "Model Predictive Control — A Simple and Powerful Method to Control Power Converters." *IEEE Transactions on Industrial Electronics* 56, no. 6 (2009): 1826–1838. https://doi.org/10.1109/TIE.2008.2008349

[13] Kwak, S., S. E. Kim, and J. C. Park. "Predictive Current Control Methods with Reduced Current Errors and Ripples for Single-Phase Voltage Source Inverters." *IEEE Transactions on Industrial Informatics* 11, no. 5 (2015): 1006–1016. https://doi.org/10.1109/TII.2015.2463757

[14] Rivera, M., J. Munoz, C. Baier, and J. Rodriguez. "A Simple Predictive Current Control of a Single-Phase Matrix Converter." In *2013 Fourth International Conference on Power Engineering, Energy and Electrical Drives (POWERENG)*, 235–239. Istanbul, Turkey: IEEE, 2013. https://doi.org/10.1109/PowerEng.2013.6635612

[15] Nguyen, M. K., Y. C. Lim, and Y. J. Kim. "A Modified Single-Phase Quasi-Z-Source AC-AC Converter." *IEEE Transactions on Power Electronics* 27, no. 1 (2012): 201–210. https://doi.org/10.1109/TPEL.2011.2157362

[16] Miranbeigi, M., H. Iman-Eini, and M. Asoodar. "A New Switching Strategy for Transformer-less Back-to-Back Cascaded H-Bridge Multilevel Converter." *IET Power Electronics* 7, no. 7 (2014): 1868–1877. https://doi.org/10.1049/iet-pel.2013.0593

[17] Liu, X., P. Wang, P. C. Loh, and F. Blaabjerg. "A Compact Three-Phase Single-Input/Dual-Output Matrix Converter." *IEEE Transactions on Industrial Electronics* 59, no. 1 (2012): 6–16. https://doi.org/10.1109/TIE.2011.2146216

[18] Alesina, A., and M. Venturini. "Solid-State Power Conversion: A Fourier Analysis Approach to Generalized Transformer Synthesis." *IEEE Transactions on Circuits and Systems* 28, no. 4 (1981): 319–330. https://doi.org/10.1109/TCS.1981.1084993

[19] Alesina, A., and M. Venturini. "Intrinsic Amplitude Limits and Optimum of 9 Switches Direct PWM AC-AC Converters." In *Power Electronics Specialists Conference, 1988. PESC '88 Record., 19th Annual IEEE*, 1284–1291, 1988. https://doi.org/10.1109/PESC.1988.18273

[20] Loh, P. C., F. Blaabjerg, F. Gao, A. Baby, and D. A. C. Tan. "Pulsewidth Modulation of Neutral-Point-Clamped Indirect Matrix Converter." *IEEE Transactions on Industry Applications* 44, no. 6 (2008): 1805–1814. https://doi.org/10.1109/TIA.2008.2006321

[21] Nguyen, T. D., and H. H. Lee. "Dual Three-Phase Indirect Matrix Converter with Carrier-Based PWM Method." *IEEE Transactions on Power Electronics* 29, no. 2 (2014): 569–581. https://doi.org/10.1109/TPEL.2013.2255067

[22] Liu, X., P. Wang, P. C. Loh, and F. Blaabjerg. "Distributed Generation Interface Using Indirect Matrix Converter in Boost Mode with Controllable Grid Side Reactive Power." In *2012 10th International Power & Energy Conference (IPEC)*, 59–64. IEEE, November 2012. https://doi.org/10.1109/ASSCC.2012.6523239

[23] Yarahmadi, A., D. A. Khaburi, and H. Behnia. "Direct Virtual Torque Control of DFIG Grid Connection Using Indirect Matrix Converter." In *2012 3rd Power Electronics and Drive Systems Technology (PEDSTC)*, 115–120. IEEE, February 2012. https://doi.org/10.1109/PEDSTC.2012.6183309

[24] Uddin, M., S. Mekhilef, M. Mubin, M. Rivera, and J. Rodriguez. "Model Predictive Torque Ripple Reduction with Weighting Factor Optimization Fed by an Indirect Matrix Converter." *Electric Power Components and Systems* 42, no. 10 (2014): 1059–1069. https://doi.org/10.1080/15325008.2014.913739

[25] Garcia, C. et al. "Predictive Current Control of a Four-Leg Indirect Matrix Converter with Imposed Source Currents and Common-Mode Voltage Reduction." In *2013 IEEE Energy Conversion Congress and Exposition (ECCE)*, 5306–5311, 2013. https://doi.org/10.1109/ECCE.2013.6647420

[26] Soeiro, T. B., T. K. Jappe, P. a. M. Bezerra, and M. L. Heldwein. "Bidirectional Delta-Switch Indirect Matrix Converter: Topologies and Modulation Strategies." In *2013 IEEE International Conference on Industrial Technology (ICIT)*, 1880–1885, February 2013. https://doi.org/10.1109/ICIT.2013.6505964

[27] Garcia, C. et al. "Predictive Current Control of a Four-Leg Indirect Matrix Converter with Imposed Source Currents and Common-Mode Voltage Reduction." In *2013 IEEE Energy Conversion Congress and Exposition (ECCE)*, 5306–5311, 2013. https://doi.org/10.1109/ECCE.2013.6647420

[28] Zhang, M., D. J. Atkinson, B. Ji, M. Armstrong, and M. Ma. "A Near-State Three-Dimensional Space Vector Modulation for a Three-Phase Four-Leg Voltage Source Inverter." *IEEE Transactions on Power Electronics* 29, no. 11 (2014): 5715–5726. https://doi.org/10.1109/TPEL.2013.2297205

[29] Rivera, M., V. Yaramasu, A. Llor, J. Rodriguez, B. Wu, and M. Fadel. "Digital Predictive Current Control of a Three-Phase Four-Leg Inverter." *IEEE Transactions on Power Electronics* 60, no. 11 (2013): 4903–4912. https://doi.org/10.1109/TIE.2012.2219837

[30] Wheeler, P., and S. Mar. "A Simple Current Control Method with Instantaneous Reactive Power Minimization for Four-Leg Indirect Matrix Converters." In *Proceedings of the 14th European Conference on Power Electronics and Applications (EPE 2011)*, 2011. https://doi.org/10.1109/epepemc.2012.6397289

[31] Uddin, M., S. Mekhilef, M. Rivera, and J. Rodriguez. "Predictive Indirect Matrix Converter Fed Torque Ripple Minimization with Weighting Factor Optimization." *The 2014 International Power Electronics Conference*, 3574–3581, 2014. https://doi.org/10.1109/IPEC.2014.6870011

[32] Rivera, M., J. Rodriguez, B. Wu, J. R. Espinoza, and C. A. Rojas. "Current Control for an Indirect Matrix Converter With Filter Resonance Mitigation." *IEEE Transactions on Industrial Electronics* 59, no. 1 (2012): 71–79. https://doi.org/10.1109/TIE.2011.2165311

[33] Rivera, M., J. Rodriguez, J. R. Espinoza, and H. Abu-Rub. "Instantaneous Reactive Power Minimization and Current Control for an Indirect Matrix Converter Under a Distorted AC Supply." *IEEE Transactions on Industrial Informatics* 8, no. 3 (2012): 482–490. https://doi.org/10.1109/TII.2012.2194159